Chapter 7

Bunsen Burner Model

7.1 Purpose of the Bunsen Type Burner Model

The Bunsen type burner with co–flow is a very simple experimental configuration that avoids many complications of modern gas turbine combustors such as complex fluid mechanics and high levels of turbulence. The laminar Bunsen flame is however a non–ideal burning environment that also shows similarities to the gas turbine combustor environment. The flame is stabilized by a delicate balance between heat–loss and fluid mechanical strain. The flame is surrounded by a shroud of dilution air that affects the burning.

The Bunsen type burner model shows that global chemiluminescence measurements can be modeled and understood using simple physical principles without detail information about the exact burning process. Through the understanding of chemiluminescence several other aspects of the burning process can be elucidated, at the very least at a qualitative level.

7.2 Modeling Approach

A Bunsen flame is illustrated in Figure 7.1 and shown in a photograph at stoichiometric conditions in Figure 7.2. The Bunsen type burner model of the flame is illustrated in Figure 7.3. Some elements of the real flame are carried over to the model, others are not. The Bunsen flame curvature is the most significant aspect neglected in the model. Every other important characteristic of the Bunsen burner flame can be represented in the model.

The cone is divided into differential segments as shown in Figure 7.3. The flame element is defined by its location relative to the burner rim both in terms of height and radius. The location of the flame element defines the heat–loss from the flame as well as the equivalence ratio of the incoming mixture for the element. The local heat–loss together with the local equivalence ratio determine the burning rate for the element via calculations using the 1-D premixed flame program PREMIX (see Section 6.1). PREMIX also allows the integration of chemiluminescence yield through

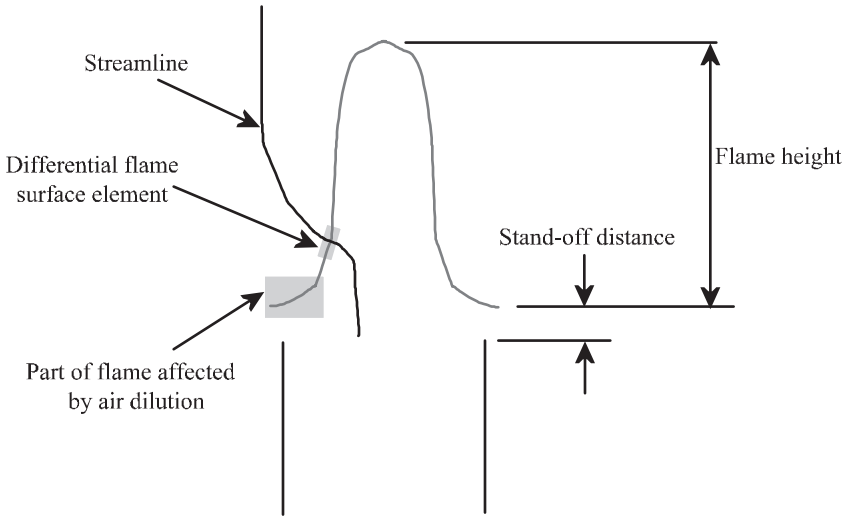

Figure 7.1: Illustration of Bunsen burner experimental flame

the differential flame element as given in Equation 6.6. The local burn–rate is integrated over the entire cone to obtain an overall burn–rate. The same integration will yield global values of chemiluminescence yield. A general form of the integration for some quantity F, distributed over the surface is given in Equation 7.1. F takes the place of the mass flow–rate per unit area, the heat–release rate per unit area or the chemiluminescence power per unit area.

$$F_{total} = \int_0^H F(\phi, q_l'')\ 2\pi R \left(1 - \frac{y}{H}\right) \sqrt{1 + \left(\frac{R}{H}\right)^2}\ dy \tag{7.1}$$

In all modeling calculations the flame base is kept constant. The height of the flame is determined by iteration. The experimental flame to be modeled has a specific fuel flow–rate. The model will iterate on the flame height until the fuel consumption of the model matches that of the experiment.

Figure 7.2: Photograph of stoichiometric Bunsen type flame

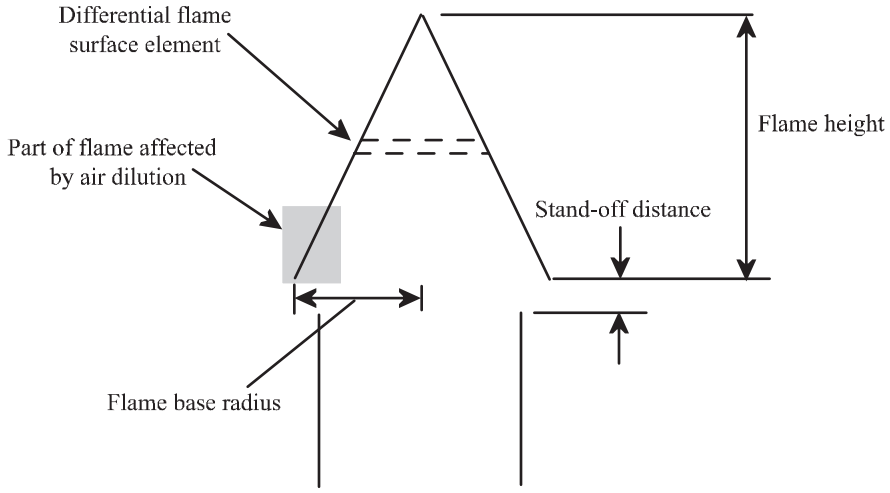

Figure 7.3: Illustration of Bunsen burner flame model

7.3 Bunsen Type Burner Model Components

To provide closure for the model, relationships between the position of the flame element and all other flame relevant quantities must be obtained. The model will translate the position into both heat–loss and local equivalence ratio using a low-order approximation of the heat–transfer and mixing observed in the flame. The local heat–loss and equivalence ratio will then determine all other flame–related quantities such as chemiluminescence yield and burn–rate through the calculations performed using PREMIX.

7.3.1 Semi-empirical mixing model

The local chemiluminescence measurements revealed that significant mixing between the co–flow of air and the main premixed fuel and air stream exists. To model the effect, a variation of the local equivalence ratio along the height of the flame is prescribed in the model. The form of the variation is given in Equation 7.2. The constants in the equation may vary with main–stream equivalence ratio. ϕ_l represents the leanest equivalence ratio at the edge of the flame. b is a parameter governing how evenly the equivalence ratio increases from ϕ_l to the main stream equivalence ratio ϕ_o. b is kept constant for all calculations at a value of 30. h_{ch} is the height at which the main stream equivalence ratio is reached. Beyond h_{ch}, the equivalence ratio does not change. The formula shown in Equation 7.2 is a crude model of the complex mixing processes that actually occur but the modeling results given in Section 7.4 will show that the model is sufficient to capture the major experimental influences of the co–flow of air. The model is termed "semi–empirical" because the variation of parameters ϕ_l and h_{ch} with equivalence ratio is determined by attempting to match modeling results to experimental data.

$$\phi_{local}(y) = \begin{cases} \frac{\phi_o - \phi_l}{e^{b h_{ch}} - 1} \left(e^{b\,y} - 1 \right) + \phi_l & \text{for} \quad y < h_{ch} \\ \phi_o & \text{for} \quad y \geqslant h_{ch} \end{cases} \tag{7.2}$$

7.3.2 Semi-empirical heat–loss model

Heat–loss from the Bunsen burner flame is by radiation and conduction. PREMIX, as used in the Bunsen burner modeling calculations does not account for radiation heat–loss. The formula given in Equation 7.3 assumes that both heat–loss by radiation and conduction are based on the flame temperature, T_{flame}. The major heat sink for the Bunsen burner flame is the stainless steel burner rim with a temperature of T_{rim}. The conductivity λ, is kept constant at a value of 0.04 W/ (m-K^o). The final parameter governing the conduction heat–loss is the stand–off distance of the edge of the flame, d_{st}. The radiation sink, T_{sink} was assumed black with temperature of 298K^o. The emissivity of the flame, ϵ is considered constant at 0.005.

$$q_l''(y) = \lambda \frac{T_{flame} - T_{rim}}{y + d_{st}} + \epsilon\sigma\left(T_{flame}^4 - T_{sink}^4\right) \tag{7.3}$$

7.3.3 PREMIX 1-D flame results

Heat–loss and local equivalence ratio determine all other flame variables such as local burn–rate, chemiluminescence and flame temperature through PREMIX calculations. PREMIX calculations were originally performed in the two–dimensional parameter space of burner flow–rate and equivalence ratio. Burner flow–rate is related directly to heat–loss, and due to the application of the PREMIX results in the Bunsen burner flame model, heat–loss is considered the independent variable.

All of the PREMIX calculations resolve the computational domain with at least 200 points to achieve the desired accuracy in the chemiluminescence species mole–fraction variation through the flame. The chemiluminescence species variation through the flame is the last to converge as the computational grid is refined because of the extremely low mole–fractions observed for the chemiluminescence species. The maximum mole–fraction for excited species is on the order of 10^{-13}.

Flame temperature

The flame temperature is defined to be the maximum temperature observed in the computational domain of the PREMIX calculation. The flame temperature is

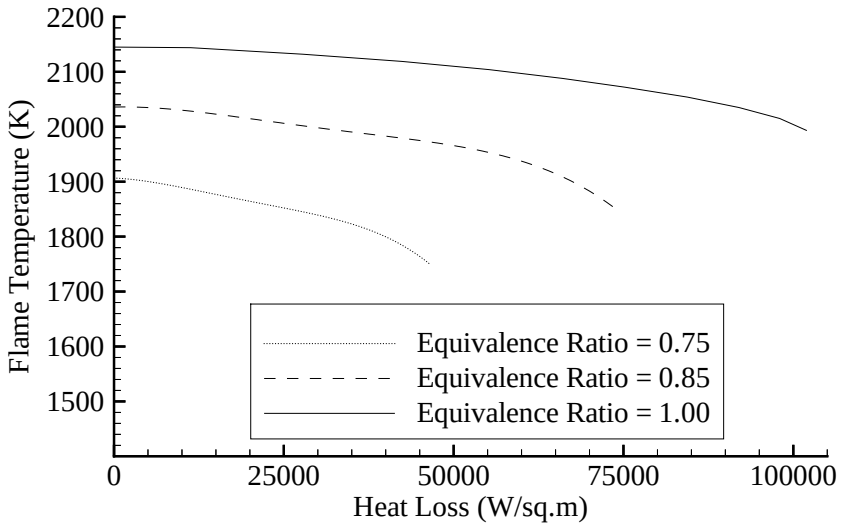

Figure 7.4: Flame temperature as a function of heat–loss

shown as a function of heat–loss for three equivalence ratios in Figure 7.4. Flame temperature is most sensitive to heat–loss at lower equivalence ratios, as can be expected due to the fact that less heat is liberated at these equivalence ratios.

Flame–speed

The flame–speed as defined here is directly related to the burn-rate per unit area by the dividing the latter by the incoming mixture density. Velocity is shown because it is a more commonly used quantity than burn–rate. The flame–speed as a function of heat–loss is shown in Figure 7.5.

7.4 Bunsen Type Burner Modeling Results

The following paragraphs present the results of the chosen parameter variation, frozen with changes in flow–rate. Results are discussed only with respect to the comparison of experimental data and modeling results of chemiluminescence mea-

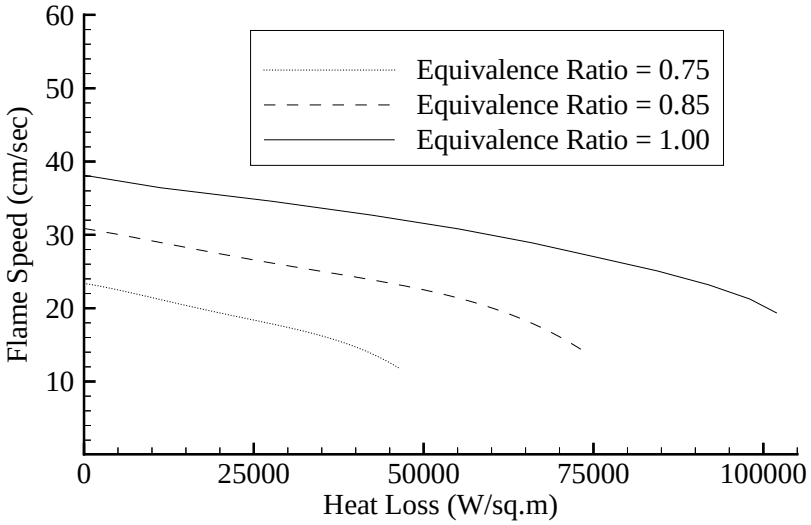

Figure 7.5: Flame–speed as a function of heat–loss

surements. Detail analysis and evaluation of chemiluminescence as a heat–release rate indicator is given in Section 10.2.1.

7.4.1 Summary of modeling procedure

Before presenting the modeling results, the procedure used to obtain these results is summarized. The parameters defined above in Section 7.3.1 and Section 7.3.2 are set by matching, to the best of the model's ability the OH^* chemiluminescence experimental data for a flow–rate of 60 cc/sec of air. The conversion factor from the units of experimentally measured chemiluminescence (cV-A) to the yield calculated in PREMIX, is determined at an equivalence ratio of 0.90 and held constant for all other data points. Once the parameter values are determined as a function of equivalence ratio for one flow–rate they are not changed for the other flow–rates.

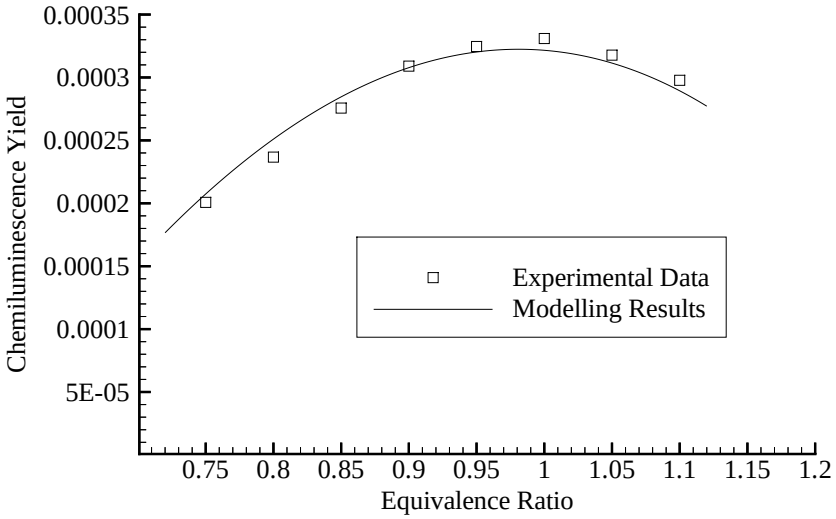

Figure 7.6: OH* modeling results and experimental data at an air flow–rate of 60 cc/sec

7.4.2 OH*modeling results

Global chemiluminescence

The global OH* modeling results at an air flow–rate of 60 cc/sec are compared to the global experimental data in Figure 7.6. The model predicts the general trend with equivalence ratio very well. Full quantitative agreement however is not achieved. The peak chemiluminescence in the model occurs at a leaner equivalence ratio than was observed in the experiment. The decline of chemiluminescence on the lean side of the equivalence ratio spectrum is steeper in the experiment than that observed in the modeling results.

The variation of the modeled global chemiluminescence with flow–rate is compared to the experimental data in Figure 7.7 for an equivalence ratio of 0.90. The apparent linear variation of chemiluminescence with flow–rate is observed for both experimental and modeling calculations. The model increase has a slightly steeper slope than the experimental data collected. Part of the reason for the model calculated steeper slope is that all parameters were frozen for variations in flow–rate.

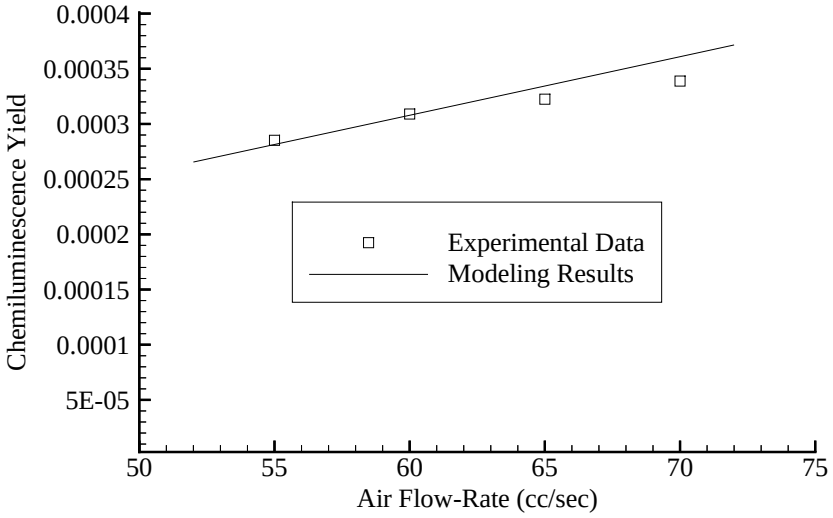

Figure 7.7: OH^* modeling results and experimental data at an equivalence ratio of 0.90

In Section 5.1.1, the collapse of the OH^* chemiluminescence experimental data was achieved using the square–root of the Reynolds number. Since the Reynolds number does not vary significantly over the experimental range studied, the square–root dependence of OH^* chemiluminescence cannot be readily identified. The modeled chemiluminescence as well would clearly show non-linear behaviour if a wider range of flow–rates were considered.

The non–linear variation of chemiluminescence is due to the mixing height which is kept constant with flow–rate and so automatically increases the average equivalence ratio closer and closer to the incoming mixture equivalence ratio. Since chemiluminescence is not a linear function of equivalence ratio, keeping the mixing height constant causes a non–linearity in the variation of OH^* chemiluminescence with flow–rate. In contrast to the experimentally observed non–linearity, the model non–linearity influence is very equivalence ratio dependent. In the model rich equivalence ratios will tend to have lower and lower per unit mass yields of OH^* chemiluminescence as the flow–rate is increased. Lean equivalence ratios will tend to have higher per unit mass yields of chemiluminescence as the flow–rate is increased.

Local chemiluminescence

Local OH^* chemiluminescence intensity as a function of the radial coordinate is shown in Figure 7.8. Shown with chemiluminescence intensity variation is the variation of the local equivalence ratio. The increase of chemiluminescence over the radius is similar in magnitude to that observed in the experimental data shown in Figure 5.8 for example. The model chemiluminescence variation is however mostly due to the variation of the local equivalence ratio over the radius of the flame. Heat losses appear only to be important in the immediate vicinity of the burner rim. Curvature effects, which contribute significantly to the shape observed experimentally are not considered in the model. Similarly, the local minimum of chemiluminescence intensity observed in the center of the flame is not observed in the model, because the diffusion and pressure influences are not considered by the model. Section 7.5.3 addresses burning at the flame center in greater detail.

It is important to reiterate that the goal of the model is not to provide a complete model of the Bunsen flame in air co–flow but rather to model the general behaviour of the flame in order to provide a basis for the interpretation of chemiluminescence measurements in terms of heat–release rate. The modeling success for global chemiluminescence shows that the level of complexity in the model is adequate to attain the goal of the model.

The units of the displayed local chemiluminescence are that of yield intensity since the values have not been integrated over the flame area to give an overall chemiluminescence yield.

7.4.3 CH^* modeling results

Global chemiluminescence

The same conversion factor used above to compare OH^* chemiluminescence experimental data with modeling results is used to compare the CH^* experimental data to the modeling results. The experimental and modeled variation of CH^* chemiluminescence is shown in Figure 7.9 for an air flow–rate of 60 cc/sec. The model captures

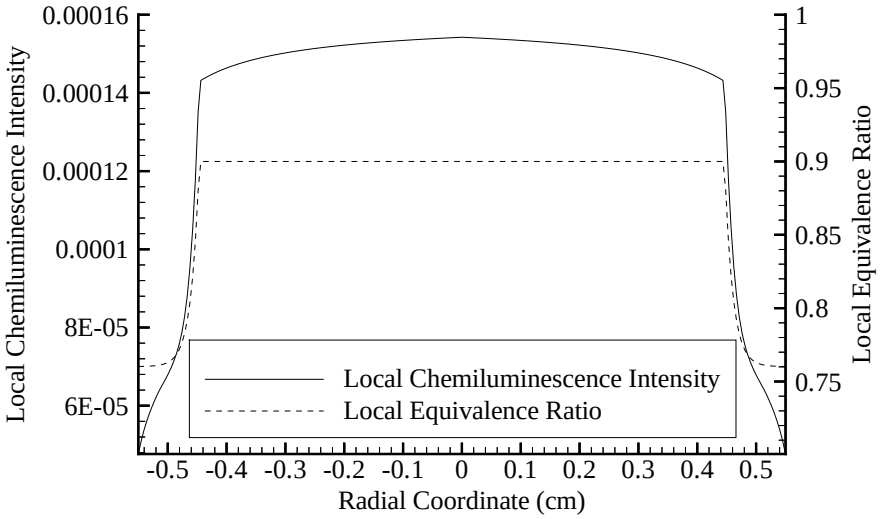

Figure 7.8: Local OH* chemiluminescence intensity modeling results at an equivalence ratio of 0.90 and an air flow–rate of 60 cc/sec

the general trend of the experimental data, especially for lean equivalence ratios. The leveling off in the CH* chemiluminescence is not observed in the model.

Figure 7.10 shows the variation of experimental and modeled CH* chemiluminescence with air flow–rate for an equivalence ratio of 0.90. As for OH* the CH* chemiluminescence variation with air flow–rate appears linear. However, in contrast to the OH* chemiluminescence results, the slope of the experimental data matches that of the modeling results much more closely. In the case of CH*, Section 5.1.1 showed that the experimental CH* chemiluminescence variation with flow–rate is indeed linear. The model however, again has a non-linear dependence of chemiluminescence on flow–rate. The reason for the non-linear dependence is the same as that for OH*, as discussed in Section 7.4.2.

Local chemiluminescence

Local CH* chemiluminescence intensity as a function of the radial coordinate is shown in Figure 7.11. Shown with chemiluminescence intensity variation is the variation of the local equivalence ratio. The increase of chemiluminescence over the

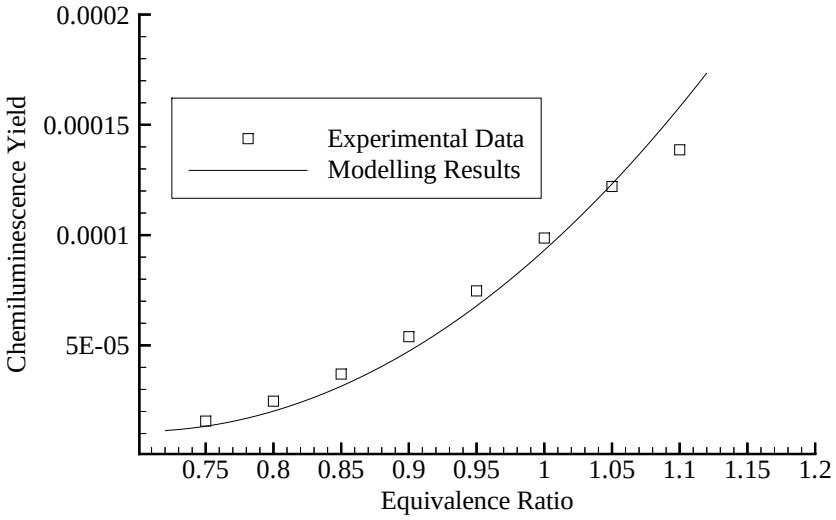

Figure 7.9: CH^* modeling results and experimental data at an air flow–rate of 60 cc/sec

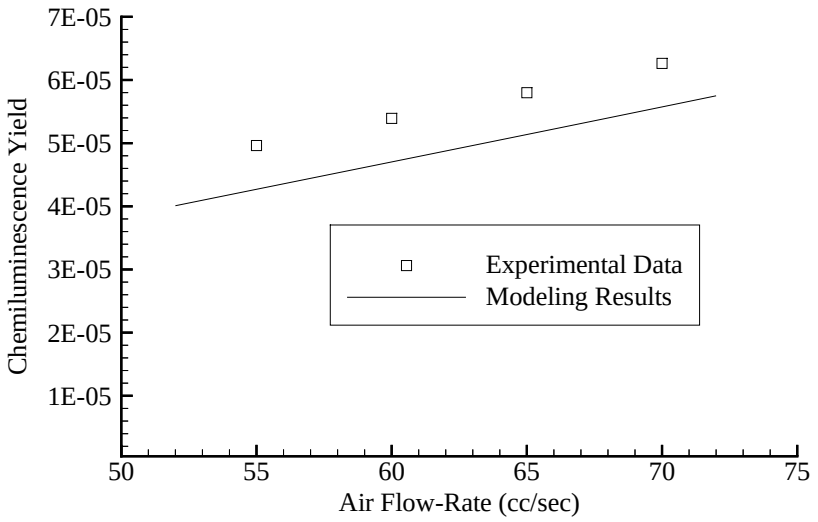

Figure 7.10: CH^* modeling results and experimental data at an equivalence ratio of 0.90

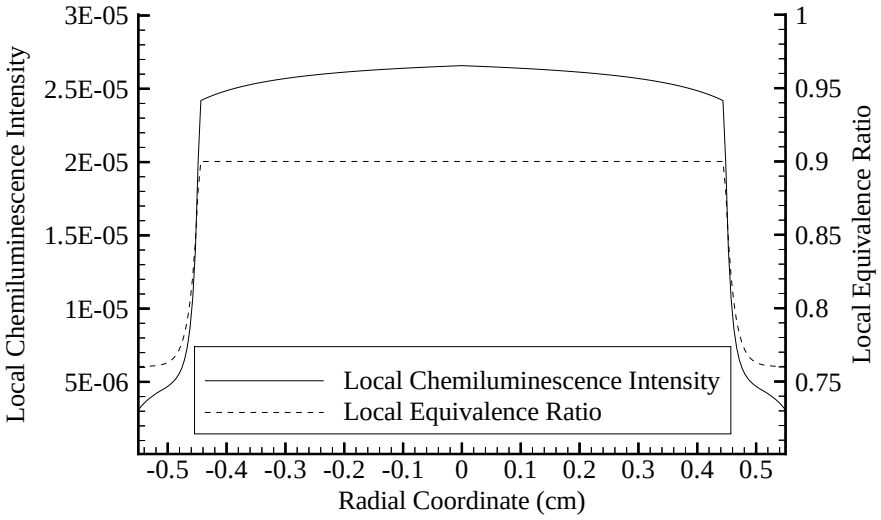

Figure 7.11: Local CH^* chemiluminescence intensity modeling results at an equivalence ratio of 0.90 and an air flow–rate of 60 cc/sec

radius is similar in magnitude to that observed in the experimental data shown in Figure 5.10 for example. As observed for local OH^* chemiluminescence, the increase in chemiluminescence intensity, except for near the burner rim, is due in great part to the equivalence ratio variation over the radius. As observed in the experimental data, there is no significant difference between the shape of the local OH^* and CH^* chemiluminescence intensity variations across the flame.

7.4.4 Chemiluminescence Ratio modeling results

Global chemiluminescence ratio

The variation of the global chemiluminescence ratio of OH^* to CH^* with main stream equivalence ratio is shown in Figure 7.12 using both experimental data and modeling results at all flow–rates. The modeled chemiluminescence ratio varied very little for variations in flow–rate, whereas there was some noticeable variation in the ratio in the experimental data. Due to the fact that the modeled CH^* chemiluminescence is lower than the experimental data for CH^* chemiluminescence, the model

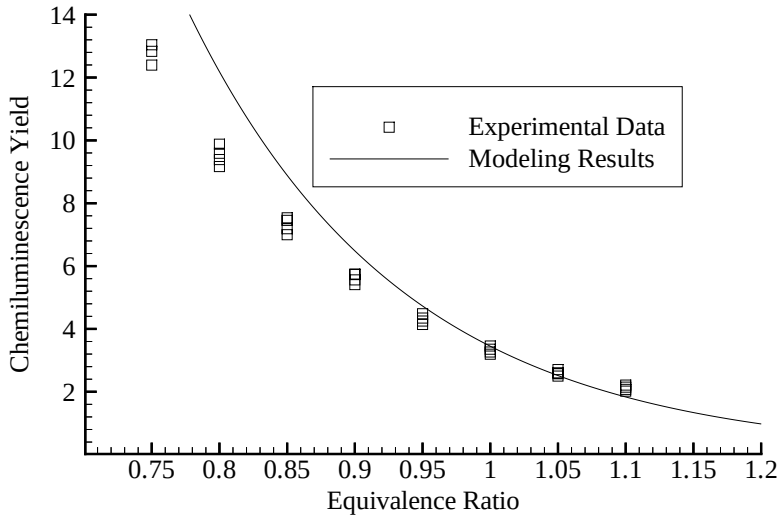

Figure 7.12: OH^* to CH^* chemiluminescence ratio modeling results and experimental data vs. mainstream equivalence ratio

chemiluminescence ratio increases more rapidly than the experimental chemiluminescence ratio for lean equivalence ratios.

Local chemiluminescence ratio

The radial variation of the modeled local OH^* to CH^* chemiluminescence ratio at an equivalence ratio of 0.9 and air flow–rate of 60 cc/sec is shown in Figure 7.13. The radial variation of the chemiluminescence ratio is very similar to the experimental results shown in Figure 5.12. The similarity shows that although the mixing model used is very crude, the model manages to capture, even locally the major influence of equivalence ratio variation. The local maximum at the flame center observed in the experimental data can however not be captured with the present model, because curvature and diffusion effects are responsible for this feature of the experimental data. Section 7.5.3 addresses burning at the flame center in greater detail.

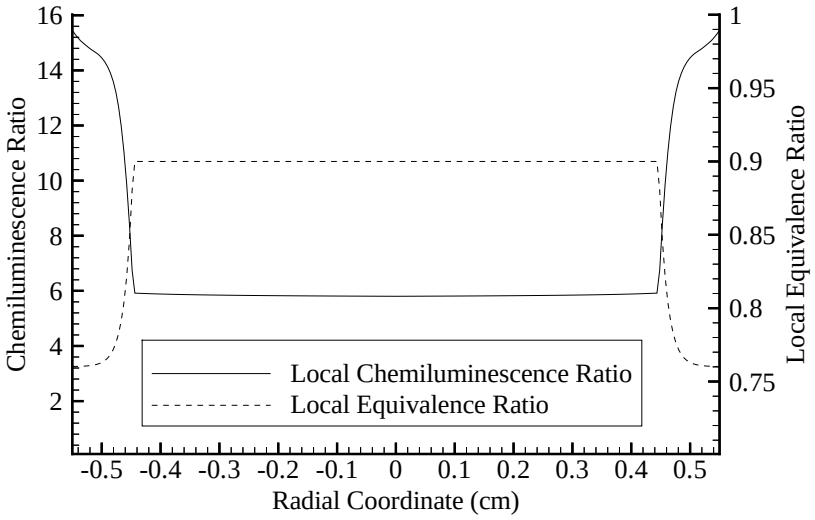

Figure 7.13: Radial variation of the modeled OH^* to CH^* chemiluminescence ratio at an equivalence ratio of 0.9 with an air flow–rate of 60 cc/sec

7.4.5 Parameter variations used

The model developed for the Bunsen burner is semi-empirical, meaning that the closure of the model was achieved using equations that contain parameters whose value is determined during the course of the modeling effort. The parameters in Equation 7.2 and Equation 7.3 are allowed to vary with equivalence ratio but not with flow–rate. An important feature of the selected parameter variations is that they are internally consistent. Higher standoff distance of the flame, for example, corresponds to a lower burner rim temperature.

Mixing parameter variation

The mixing parameter variation is shown in Figure 7.14. The mixing parameter ϕ_l is replaced in the figure by the difference between mainstream and flame edge equivalence ratio, showing more clearly the amount of mixing occurring for each equivalence ratio. The mixing height shown is the actual height in centimeters to which some mixing effects are seen. For an equivalence ratio of 0.75, the mixing height

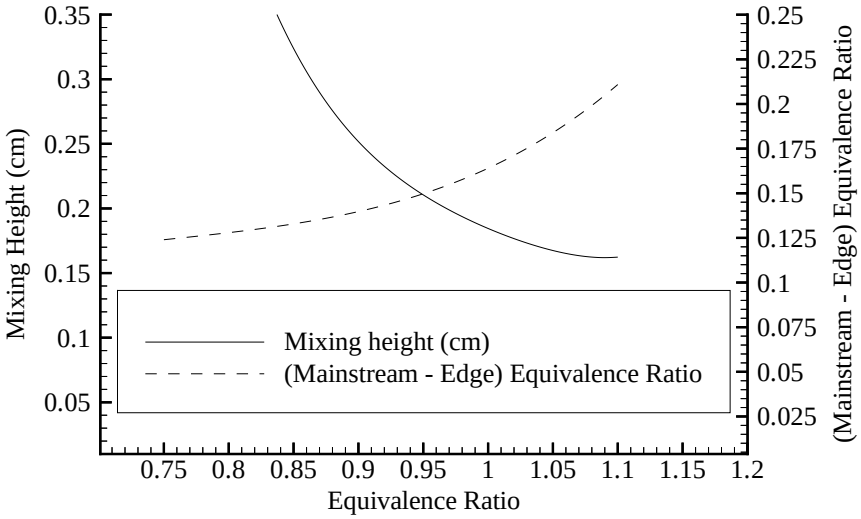

Figure 7.14: Variation of mixing parameters with mainstream equivalence ratio

shown corresponds to about 30% of the total flame height. The percentage of the total height of the flame affected by mixing is also a decreasing function of equivalence ratio. As the mixing height decreases, the difference between the mainstream and flame edge equivalence ratio increases because a smaller amount of mainstream mixture is presumed to mix with a nearly equal amount of co–flow air.

As mentioned in Section 7.4.1, all parameters were frozen for increases in flow–rate. The assumption that the mixing is not a function of flow–rate is very difficult to defend in light of the fact that the mixing is partly shear–layer driven. The use of scaling relationships, for example with the square–root of Reynolds number, was considered but dropped because it was found that the scaling of these parameters only had a very negligible effect on the modeling results. Additionally, the influence of the altered mixing environment on the thermal parameters is difficult to understand. To maintain the model's low-order character, it was decided to neglect flow–rate variation effects. In a study with a wider range of flow–rate changes in the mixing due to changes in flow–rate must be considered in the modeling effort in order to adequately capture experimental data trends.

Thermal parameter variation

The heat–transfer parameter variation is shown in Figure 7.15. The standoff distance of the flame is seen to increase almost exponentially, approaching the blow–off equivalence ratio near 0.7. Concurrently, the rim temperature decreases steeply as the blow–off point of the flame is approached. Recalling Figure 7.14, the mixing height is proportional to the standoff distance of the flame which also is intuitively correct. As the flame moves away from the burner rim, more of the mainstream mixture is allowed to mix in the shear–layer with the air co–flow. At the same time the difference between the mainstream equivalence ratio and flame edge equivalence ratio is slowly decreasing because of the increased participation of mainstream mixture in the mixing process.

On the rich side, as the flame edge equivalence ratio approaches a constant value, the rim temperature and standoff distance also approach a constant value. The temperatures and standoff distances used are not based on the CFD calculation described in Section 7.5.3 but rather are guided by measurements performed on a very similar burner by Sun et al. (1994) using interferometry in an attempt to adiabatically stabilize a Bunsen type flame.

7.5 CFD Model of Bunsen Type Burner

7.5.1 Purpose of CFD model

The purpose of the CFD model of the Bunsen type burner is to elucidate the flow structure near the flame–tip. The local chemiluminescence results shown in Section 5.1.2 show a peculiar local minimum of chemiluminescence in the center of the flame, the flame–tip. Numerical simulations by Poinsot et al. (1992) confirms the existence of a wake–type velocity profile above the flame–tip thought to be responsible, together with some diffusion effects, for the fact that the mass–flux through the flame–tip is reduced. In the present CFD model the previously mentioned wake–type velocity profile and reduced mass–flux across the flame tip is investigated to provide

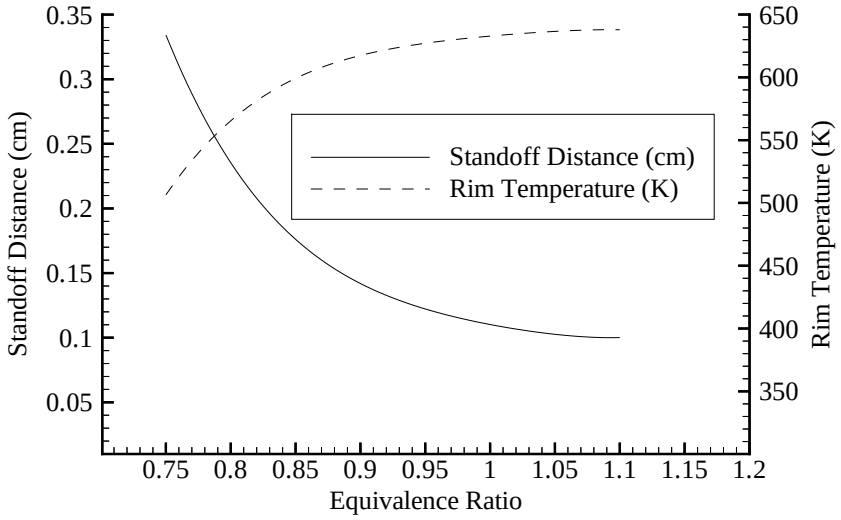

Figure 7.15: Variation of heat transfer parameters with mainstream equivalence ratio

a further physical foundation for the observed chemiluminescence variation in the flame–tip region.

7.5.2 FLUENT implementation of Bunsen type burner model

The procedure used to obtain the results shown in Section 7.5.3 was outlined in Section 6.3. The present section discusses the geometry used in the calculation. The geometry used is shown in Figure 7.16. The computational domain extends from the base of the stainless steel flame holder to the end of the long quartz chimney. At the inlets, a flat velocity profile is used with the velocity magnitude calculated based on the area–average for the given inlet. The center inlet is the premixed gas inlet where the velocity is set to 86 cm/sec to model an air flow–rate of 60 cc/sec and an equivalence ratio of 1.00. The annular air co–flow inlet velocity magnitude is constant for all conditions at 2.9 cm/sec. The stainless steel flame holder is modeled in its entirety with heat conduction within the stainless steel and heat exchange both to and from the surrounding fluid. The stainless steel tube is considered thermally insulated at its upstream end.

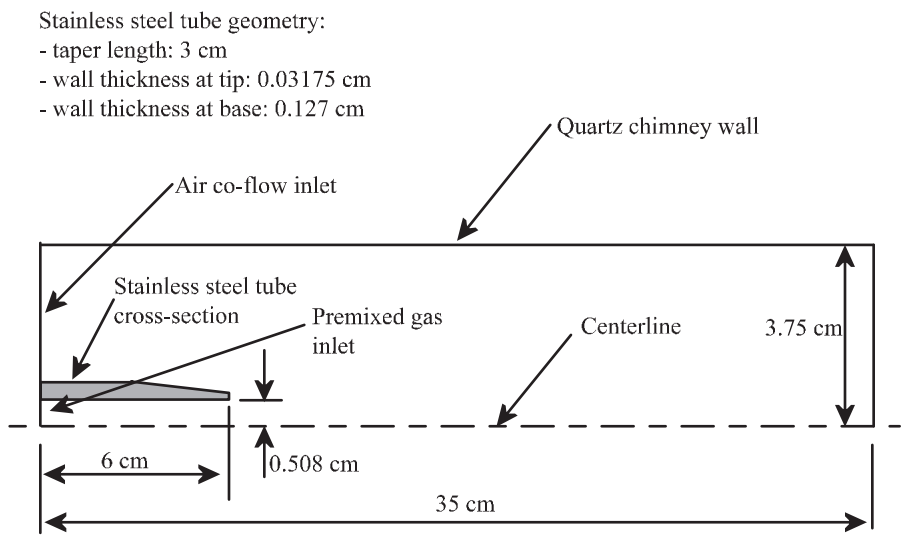

Figure 7.16: Schematic of CFD geometry for Bunsen type burner

The calculation is performed under the assumption of laminar flow. The methane reaction mechanism used consists of the Fluent default two–reaction model. The first reaction step is a reaction between methane and molecular oxygen to give carbon monoxide and water. The second reaction step is a reaction between carbon monoxide and molecular oxygen to give carbon dioxide and water. The physical properties of all gases, including viscosity, are a function of temperature. For viscosity and conductivity however, values of air only are used, i.e. gas properties are assumed identical to those of air. All other properties, including diffusion and heat–capacity are calculated for each species separately using a polynomial fit in temperature or molecular theory. The gas average coefficient, when appropriate, is calculated on a mass basis. For more information, the Fluent manuals (Fluent Inc., 1998) offer great detail in the origin and correct use of the correlations and reaction mechanisms already included in the software and used in the present investigation.

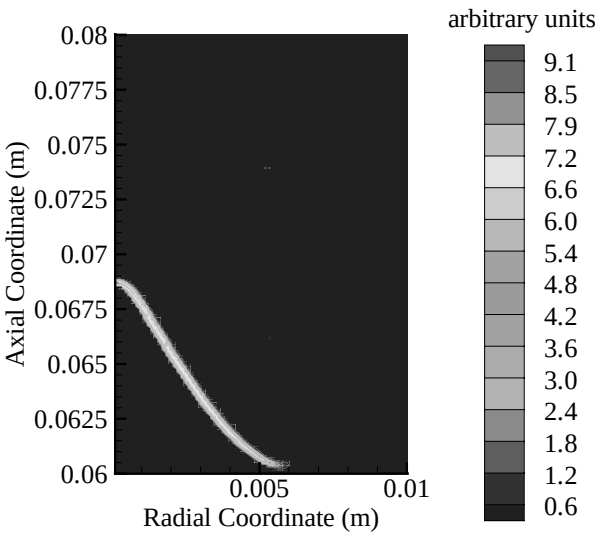

Figure 7.17: Contour plot of the methane consumption reaction rate in Bunsen type burner CFD simulation

7.5.3 Results of FLUENT Bunsen type burner model

The flame–tip wake phenomenon observed by Poinsot et al. (1992) is also found in the presently described CFD investigation. Figure 7.17 shows a contour plot for the rate of the first reaction. The outline of flame can thus be easily identified. The contour plot clearly shows that the reaction rate, as expected, is highest at the flame–tip. The contour plot also allows the flame base radius to be quantified along with the flame stand–off distance from the burner rim. The flame base diameter is only slightly larger than the stainless steel flame–holder inside exit diameter which is not surprising considering that the CFD calculation suggests that the flame stand–off distance is only 0.5 mm. The calculation also shows the significant curvature variation along the Bunsen burner flame front. The flame has a stabilizing concave curvature near the flame–tip and a flame de–stabilizing convex curvature near the flame base.

The axial velocity contour plot is shown in Figure 7.18. The plot shows the velocity deficit region immediately above the flame tip, confirming the results by Poinsot et al. (1992). Note that the tip velocity is very high, about an order of magnitude above the adiabatic flame–speed. However, the gases exhibiting the high velocity are

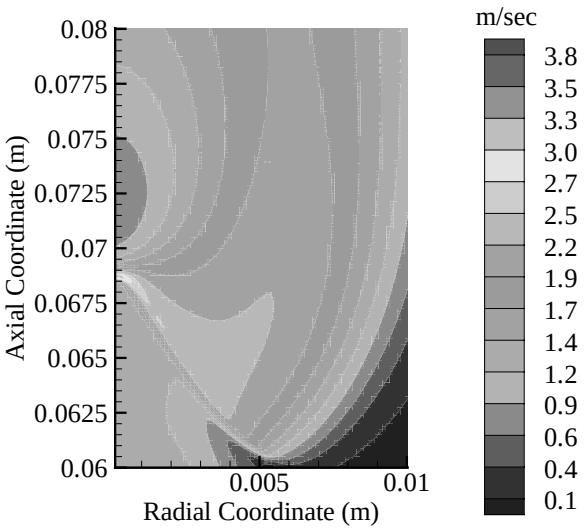

Figure 7.18: Contour plot of axial velocity in Bunsen type burner CFD simulation

not close to the inlet temperature but have experienced significant heating from the surrounding flame–sheet. The high velocity is thus a better indicator of high temperature than high mass-flow. Indeed, the analysis by Poinsot et al. (1992) showed that very little of the fuel originally contained in the center stream–tube is actually burned in the flame center. Most of the fluid is pulled away by the surrounding flame sheet through both diffusion and hydrodynamic effects. The fuel deficit in the flame center influences the local chemiluminescence yield. The chemiluminescence profiles shown in Section 5.1.2 confirm that less fuel is burned in the flame center as both OH^* and CH^* exhibit local minima in the flame center. Furthermore, the fuel diffusion effect can be deduced from the measured chemiluminescence ratio in the flame center. The ratio of OH^* to CH^* is seen to increase in the flame center leading to the conclusion that the combustion in this part of the flame is leaner than the mean equivalence ratio.

The high–velocity in the flame center has the added consequence of bringing with it a pressure minimum at the flame tip. The pressure minimum causes the flow in the center stream–tube to experience an adverse pressure gradient, thus generating the wake–like flow profile above the flame tip. The stream–lines are shown in Figure 7.19

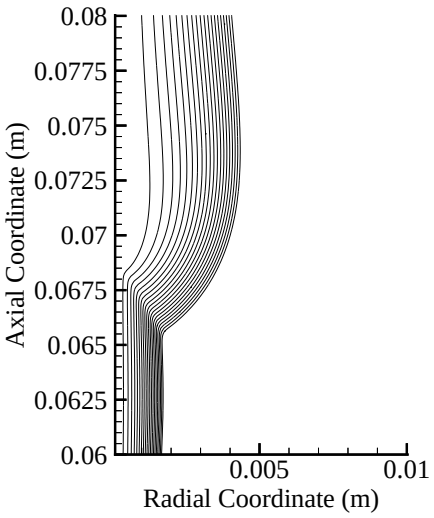

Figure 7.19: Streamlines in the Bunsen type burner CFD simulation

and also give evidence of the velocity minimum seen in Figure 7.18. The stream–lines above the flame–tip expand which can only be the result of a velocity decrease.

The axial velocity profile in the center of the wake is shown in Figure 7.20. The minimum velocity in the center of the wake is slightly more than a third of the maximum velocity. Furthermore, the minimum velocity of 0.75 m/sec means that the flow in the center stream tube has slowed by a factor of 5. An interesting consequence of the observed wake–profile is that the flow above the flame–tip is unstable considering the Rayleigh's inflection point rule. Although some unsteady calculations were performed and no unsteadiness was found, the effort was not exhaustive. The wake–profile above the flame–tip is not the only location where the flow is unstable. Another area of possible instability is the shear–layer between the air co–flow and the main premixed–gas stream. The issue of flow stability and its influence on combustion in flames will not be discussed further in this report, however, the issue is of very high importance in most industrial gas turbine combustors due to the highly turbulent nature of the flows encountered in those combustor geometries.

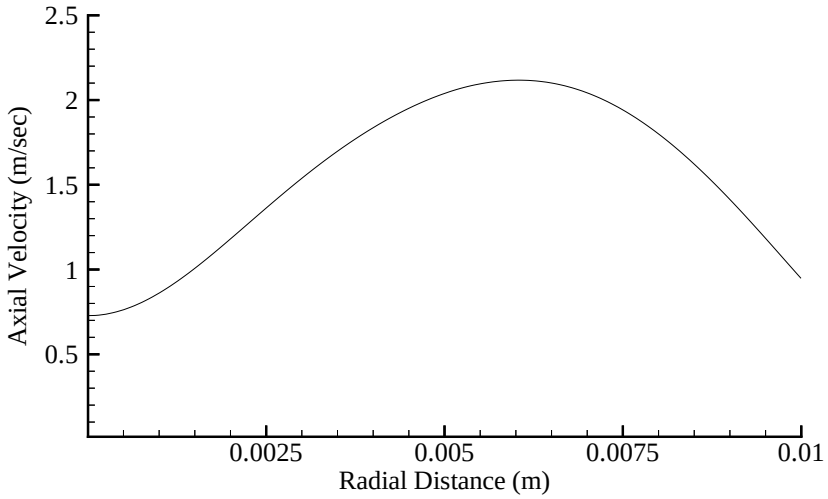

Figure 7.20: Radial velocity profile through center of wake region in the Bunsen type burner CFD simulation